Effect of Particle Size on the Dispersion of Dust Produced by a Shock Wave

Orlando J. Ugarte, Ryan W. Houim and Elaine S. Oran
University of Maryland
College Park, Maryland, USA

1 Introduction

Granular materials, which consist of fine-grained particles, occur frequently in industrial activities, such as coal mining, food processing and grain storage. The accumulation of reactive dust, however, may severely enhance the damage produced by an explosion. Explosions generate shock waves that propagate dispersing dust accumulated and suspended in mine shafts, dust conveyors, grain elevators, etc. As a result, dispersed reactive particles may ignite in the shocked-heated gas, causing a secondary explosion [1], [2]. The release of energy in the secondary explosion strengthens the shock propagation, which further intensifies the dust dispersion and particle ignition [2] and thus produces a positive feedback between the shock dispersion and the energy released by the dispersed dust. Combustion of dispersed dust can propagate at around 1000 m/s, generate pressures over 10 atm, and potentially transition to detonation [2], [3]. The improvement of safety procedures to mitigate dust explosions rely on the physical understanding of shock-particle interactions and, in particular, on understanding the dispersion of dust produced by shock waves.

The shock-dust interaction is a complex multiphase process that involves a wide range of temporal and spatial scales. The specific interaction depends on the materials, particle concentration and geometry, among other parameters. One of the systems that has attracted most research attention is the propagation of a shock through a channel containing a dust layer settled on the floor. This system is, for example, a model for the shock-dust interaction in coal mines. Early shock-tube investigations of this system showed that the shock front curves as it interacts with the dust layer [4] and that the dispersion of dust is driven by the strong flow gradients produced behind the shock [5]. Recent experimental studies identified two stages of the dust dispersion: first, a fast rise of particles occurring immediately behind the shock, followed by a second stage where the dust lifting plateaus [6]. A numerical study identified the formation of a compaction wave in the dust layer after the passage of a shock [7]. The study showed that the compaction wave reflects off of the channel floor, producing a jet-like effect on the disperse particles.

Some controversy has risen regarding the effect of the particle size on dust dispersion. It has been shown experimentally that smaller particles lead to higher dispersion in early times [8], but larger particles rise

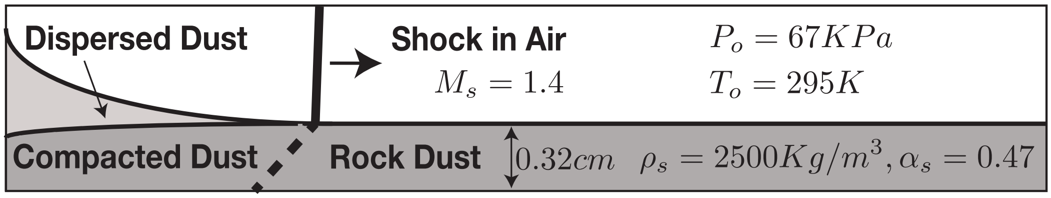

Figure 1: Schematic of shock wave propagating on top of and through a dust layer in a channel

higher at later times [9]. As a result, contradicting conclusions respect to whether larger or smaller particles lift higher have been obtained. Also, strong inter-particle forces develop in the dust-shock interaction, agglomerating particles and making it difficult to determine the effective size of particles in experiments [10]. The purpose of this paper is to investigate the effect of particle size on the dispersion of dust produced by a shock. Specifically, we consider a 325 cm long, 10 cm hight channel where a shock, initially placed 5 cm from the left boundary, propagates towards the right. Limestone dust made of uniform-size particles is initially resting on the floor. The system is shown in Fig.1. This study considers two different cases, one with 20 μm diameter particles and another with 80 μm diameter particles.

2 Methodology

The gas-dust interaction problem is solved with an Eulerian, unsteady, multidimensional numerical model [11] in which two sets of Navier-Stokes equations, one for the gas and one for the particles, are coupled by terms describing the gas-particles interaction. The set of equations for the solid particles is derived from kinetic theory of granular flow [12], and is valid for dilute and dense particle concentrations. The governing equations are solved numerically by an operator-splitting approach, which treats the hyperbolic and source terms separately. The solution algorithm uses a high-order Godunov-based technique to solve the hyperbolic terms and a third-order Runge-Kutta method for time advancement. Grid resolution is achieved by adaptive mesh refinement using the Paramesh library. Details of the model and its solution are discussed in [11].

We identify the forces controlling the particle motion from the conservation of momentum of the solid phase. These forces, listed in Table 1, are used to analyze the particle dynamics behind the shock and the mechanisms controlling the particle dispersion.

Table 1: Forces acting on dust particles

Force	Formula (N/m^3)	Description
Archimedes Force	$-\alpha_s \nabla p_g$	Due to gas pressure forces pushing on particles.
Intergranular Stress	$\nabla p_s + \nabla p_{\text{fric}}$	Due to particle collisions and frictional stress.
Gravitational	$\alpha_s \rho_s \boldsymbol{g}$	Weight per unit volume of the particles.
Lift	$C_l \alpha_s \rho_g (\mathbf{v}_s - \mathbf{v}_g) \times (\nabla \times \mathbf{v}_g)$	Due to gas shear, acting perpendicularly to $\mathbf{v}_g - \mathbf{v}_s$.
Drag	$K_{sg}(\mathbf{v}_g - \mathbf{v}_s)$	Acts along the direction of $\mathbf{v}_g - \mathbf{v}_s$.

Where α, ρ, p, $\mathbf{v}$ are the volume fraction, density, pressure and velocity, respectively. The subscript ($_s$) determines the solid phase, whereas ($_g$) determines the gas phase. The friction pressure p_{fric} adds to the solid pressure for high particle concentrations ($\alpha_{s,crit} > 0.5$ in this study). Moreover, C_l and K_{sg} are the lift and drag coefficients, respectively. The drag coefficient K_{sg} becomes smaller for larger particles. The solid pressure (p_s) is also modified by particle size, although the effect of particle size on p_s is highly non-linear.

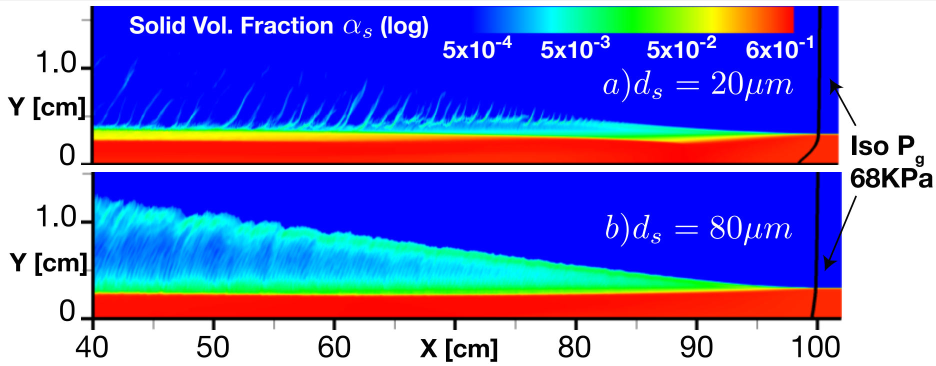

Figure 2: Variation of solid volume fraction behind a shock for 20 μm and 80 μm particles.

3 Results and Discussion

We now compare the dust dispersion produced behind the shock when the dust layer is made of two different particle sizes. Fig. 2a and Fig. 2b shows the solid volume fraction for 20 μm and 80 μm particles, respectively. These figures indicate that the dust is more dispersed for larger particles. These results are consistent with experimental observations [9]. The passage of the shock increases the solid volume fraction from α_s = 0.47 (the dust concentration ahead of the shock) to around 0.60. This indicates that the shock not only disperses particles, but also compacts the dust layer. The dust layer is more distorted for 20 μm particles than for 80 μm particles, as indicated by the indentation in the dust layer surface around 90 cm in Fig. 2a. Another difference between the two cases is the curvature of the shock wave, indicated by the isothermal p_g = 68 KPa at 100 cm, which shows that the shock is more curved when smaller particles form the dust layer.

More information about the particle dynamics behind the shock is presented in Fig. 3, which shows the vertical acceleration of particles for the two particle sizes. The particle acceleration is the result of the combined effect of the forces listed in Table 1. The figure shows an alternating positive - negative acceleration of the dispersed dust in the two cases. The alternating pattern indicates that the dispersed particles accelerate upwards and downwards, following an oscillatory flow motion. Moreover, the compaction of particles in the dust layer produces a compaction wave that later reflect off of the channel. For 20 μm particles, the compaction wave reflects nearer to the shock than for 80 μm particles. The reflection of the compaction wave for 20 μm particles coincides with the starting of the oscillatory motion of the dispersed particles. For the 80 μm particles, however, the oscillatory motion of the dispersed particles does not start with the reflection of the compaction wave, but much earlier.

Figure 4 shows vertical particle-accelerations produced by each of the forces listed in Table 1. The computations are performed on selected locations in the dust layer and the dispersed dust. For the dust layer, we select particles along a horizontal line located at Y = 0.15 cm, which is 0.17 cm below the initial layer thickness (indicated in Fig. 4a by a dashed line). For the dispersed dust, we select the particles located at the edge of the dispersed cloud, which are indicated in Fig. 4a for the two particle sizes. Figures 4b and 4c show the results inside the dust layer for 20 μm and 80 μm particles, respectively. The figures show that Archimedes and drag forces accelerate particles downwards near the shock, which as in Figs. 2 and 3 is located at 100 cm. The intergranular stress shows large pick values for the two particle-size cases. The location of the pick values correspond to the locations where the reflection of the compaction wave occurs, namely around 90

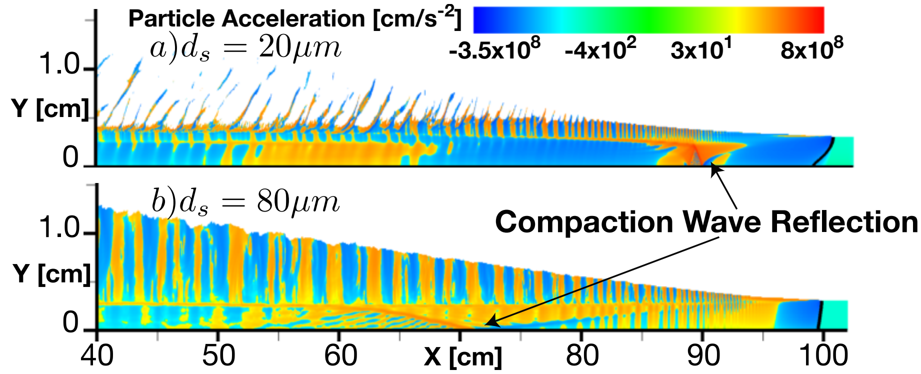

Figure 3: Vertical component of particle acceleration behind a shock, for 20 μm and 80 μm particles.

cm for 20 μm particles and near 70 cm for 80 μm particles. Notice that the pick acceleration produced by intergranular forces is one order of magnitude larger for 20 μm than for 80 μm particles.

Computations at the edge of the dispersed dust, Fig. 4d and 4e, show that the upward acceleration driven by intergranular and lift forces on 20 μm particles is much larger than for 80 μm particles. However, the downward acceleration driven by drag is also larger for 20 μm particles than for 80 μm particles. For a given volume of a gas-particle mixture, the total surface of the particles is larger for smaller particles, leading to a larger drag from the gas-phase flow. Therefore, even though 20 μm particles experience larger upward acceleration than 80 μm particles, the 20 μm particles also experience much larger drag, resulting on a smaller net upward-acceleration for 20 μm particles. This explains why 80 μm particles are more dispersed in Fig. 2.

4 Conclusions

A two-fluid model is used to study the effect of particle size on the dust dispersion produced by a shock. Namely, we simulate the propagation of a shock wave (M_s = 1.4) through a layer of limestone dust, which initial height and volume fraction are 0.32 cm and 0.47, respectively. The dust layer is made of uniform-size particles. This investigation focus on two cases, given by dust layers made of 20 μm and 80 μm particles.

The dust dispersion is studied by evaluating the vertical component of the forces acting on the particles. These forces are the Archimedes force, produced by gas pressure gradients, drag and lift forces, produced by the relative motion between particles and gas, intergranular forces, which result from particle collisions and frictional stress, and the gravitational force.

The propagating shock compacts and disperses the dust layer for the two particle-size cases. The dust layer made of 80 μm particles disperse higher than the dust layer made of 20 μm particles. The shock curves as it interacts with the dust layer. The shock curvature is larger for 20 μm particles than for 80 μm particles.

Drag and Archimedes forces compact the dust layer in the two cases. The compaction evolves to a compaction wave which later reflects off of the channel. The reflection of the compaction wave occurs nearer to the shock for 20 μm particles than for 80 μm particles.

The acceleration produced by intergranular and drag forces are larger for 20 μm particles than for 80 μm particles, whereas lift-driven acceleration remains almost the same. Even though 20 μm particles experience

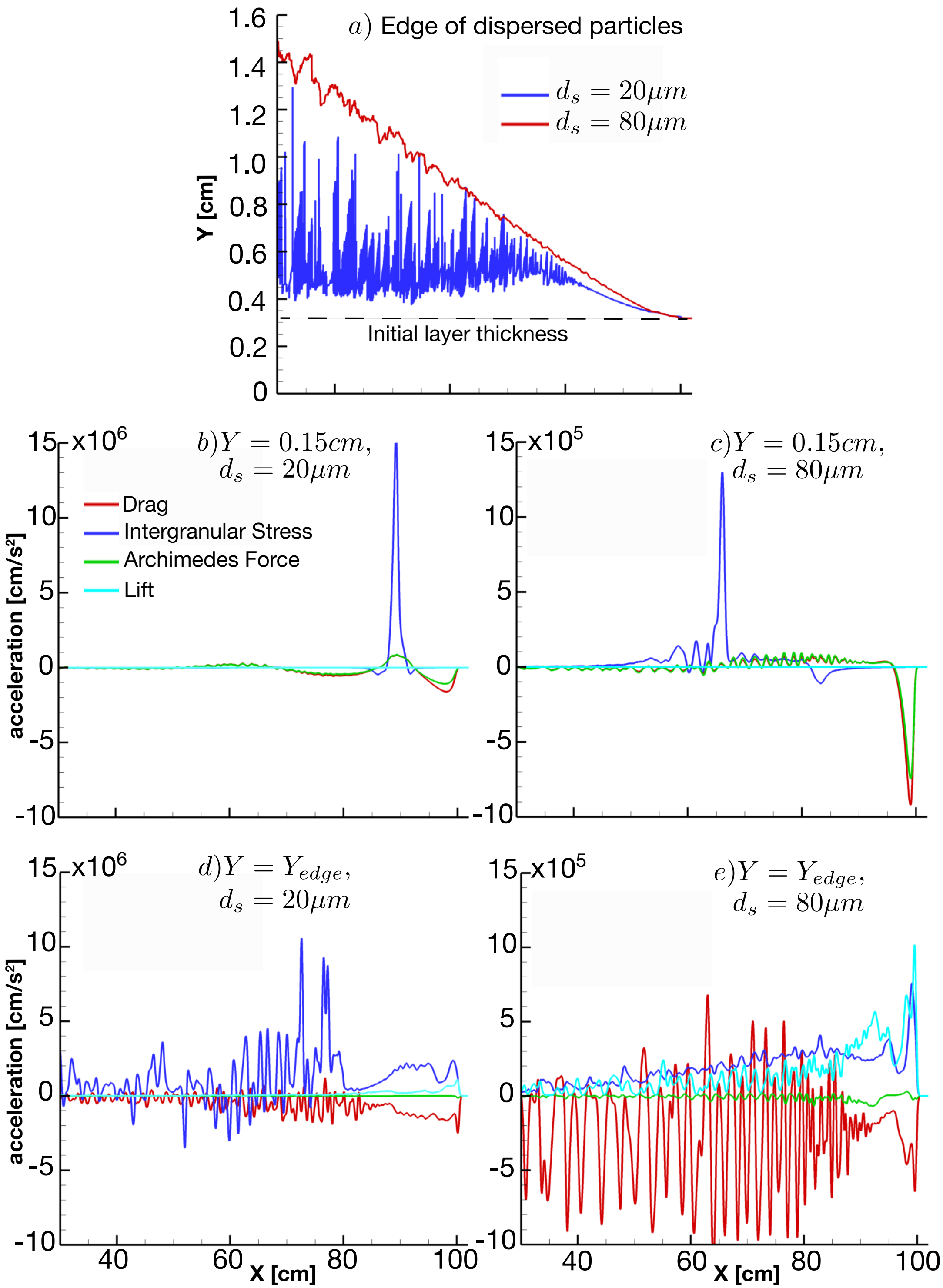

Figure 4: Height of the dispersed dust for 20 μm and 80 μm particles (a). Computation of forces listed in Table 1 inside the dust layer at Y = 0.15 cm (b, c) and at the edge of the dispersed dust (d, e).

larger acceleration upwards, the drag opposing particle lifting for 20 μm particles is much larger than for 80 μm particles. As a result, 80 μm particles disperse higher than 20 μm particles.

5 Acknowledgements

This work was supported by the National Institute for Occupational Safety and Health. The authors acknowledge the University of Maryland supercomputing resources (http://www.it.umd.edu/hpcc) made available in conducting the investigation presented in this extended abstract.

References

[1] Eckhoff RK. (2003). Dust explosions in the process industries. Elsevier (ISBN 0-7506-7602-7).

[2] Houim RW, Oran ES. (2015). Numerical simulation of dilute and dense layered coal-dust explosions. Proc. Combust. Inst. 35: 2083.

[3] Li Y, Harbaugh A, Alexander C, Kauffman C, Sichel M. (1995). Deflagration to detonation transition fueled by dust layers. Shock Waves 5: 249.

[4] Gerrard JH. (1963). An experimental investigation of the initial stages of the dispersion of dust by shock waves. British J. Applied Physics 14: 186.

[5] Fletcher B. (1976). The interaction of a shock with a dust deposit. J. Phys. D: Applied Phys. 9: 197.

[6] Chowdhury AY, Johnston HG, Marks B, Mannan MS, Petersen EL. (2015). Effect of shock strength on dust entrainment behind a moving shock wave. J. Loss Prevent. Proc. 36: 203.

[7] Houim RW, Ugarte OJ, Lai S, Oran ES. (2016). Mechanisms of dust scouring behind shock waves. Proc. 11th Int. Symposium on Hazards, Prevention and Mitigation of Ind. Explosions

[8] Suzuki T, Adachi T. (1984). The effects of particle size on shock wave-dust deposit interaction. Proc. 14th Int. Symposium on Space Tech. and Science.

[9] Hwang CC. (1986). Initial stages of the interaction of a shock wave with a dust deposit. Int. J. Multiphase Flow 12:655.

[10] Johnston H, Chowdhury A, Mannan M, Petersen E. (2016). Effect of coal-limestone mixtures on dust dispersion behind a moving shock wave. Journal of Loss Prevention in the Process Industries 44: 551.

[11] Houim RW, Oran ES. (2016). A multiphase model for compressible granular-gaseous flows: formulation and initial tests. J. Fluid Mechanics 789: 166.

[12] Gidaspow D. (1994). Multiphase flow and fluidization. Academic Press (ISBN 0-12-282479-9).